

# Quantum-torque-induced breaking of magnetic domain walls in ultracold gases

A. Farolfi, A. Zenesini\*, D. Trypogeorgos†, C. Mordini, A. Gallemí, A. Roy, A. Recati\*, G. Lamporesi\*, and G. Ferrari  
*INO-CNR BEC Center and Dipartimento di Fisica, Università di Trento,*  
*and Trento Institute for Fundamental Physics and Applications, INFN, 38123 Povo, Italy.*  
 (Dated: November 10, 2020)

A rich variety of physical effects in the spin dynamics arises at the interface (domain wall) between different magnetic materials [1]. Engineered physical systems based on magnetic interlaced structures have received wide interest in the last years as a starting point to implement spin transistors, memories and other spintronic devices [2, 3]. In this work, we use a coherently-coupled mixture of ultracold bosonic gases to realize analogues of magnetic junctions. The spatial inhomogeneity of the atomic gas makes the system change its behavior from regions with oscillating magnetization, resembling a magnetic material in the presence of an external transverse field, to regions with a defined magnetization, as in magnetic materials with a ferromagnetic anisotropy stronger than external fields. Starting from a far-from-equilibrium fully polarized state, magnetic domain walls form spontaneously. We observe that the so-called quantum torque causes the breaking of such domain walls and the accumulated energy is released into short-wavelength magnetic waves that propagate in the system. Our results provide a novel platform for the study of far-from-equilibrium spin dynamics, free from dissipation and in regimes that are not easily accessible in solid-state systems.

The local magnetization in a magnetic material evolves depending on three ingredients: the external magnetic field, the nonlinear ferromagnetic anisotropy and the inhomogeneity of the magnetization itself. The evolution can be described by using the well known Landau-Lifshitz equation (LLE) [4, 5]. When a large external magnetic field is applied, all spins precess around it. For a vanishing field amplitude, the spins precess around a preferential spatial direction characteristic of the material itself, given by the magnetic anisotropy. In real materials, this anisotropy is usually very small compared to the lowest technically achievable uniform external field. The term of the LLE incorporating the inhomogeneity – derivable from the Heisenberg exchange term – becomes particularly relevant in the presence of magnetic interfaces. In the absence of such an exchange term, the LLE reduces to the Josephson equations for Bose-Einstein condensates [6, 7]. Similarly to a magnet in an external field, Josephson equations have different dynamical regimes: either the system oscillates between two states (precession around external field) or it is self-trapped in one of them (precession around dominant anisotropy direction).

In our experiment, we coherently couple two hyperfine states,  $|F, m_F\rangle = |1, \pm 1\rangle$ , of ultracold  $^{23}\text{Na}$  atoms, trapped in an elongated harmonic potential (see Methods);  $F$  is the total atomic angular momentum and  $m_F$  is its projection along the quantization  $z$  axis. This system is equivalent to a magnetic material with nonuniform magnetic anisotropy in the presence of an external transverse field, as sketched in Fig. 1. In the analogy, the effective external magnetic field is represented by the electromagnetic radiation that coherently couples the spin states, while the ferromagnetic anisotropy is due to the nonsymmetric interatomic interactions and varies spatially thanks to the density inhomogeneity of the sample. If all spins are initially aligned along  $z$  and a field is suddenly applied, they start precessing, as illustrated by

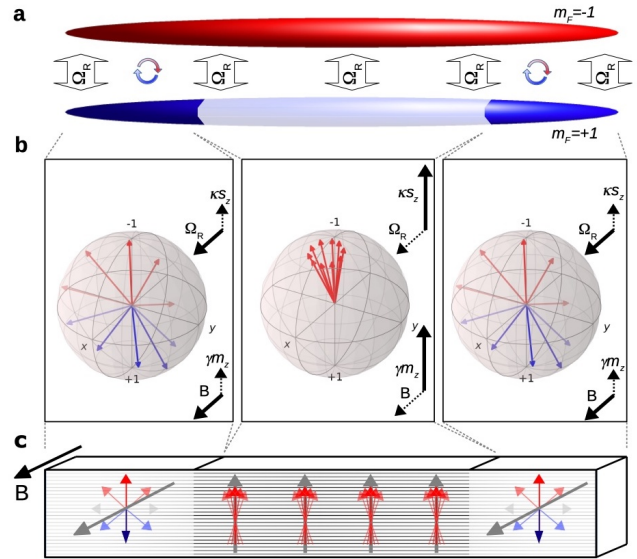


FIG. 1. **Analogy between a coherently-coupled atomic mixture and a magnetic heterostructure.** **a**, Sketch of the trapped ultracold atomic mixture in the two hyperfine states  $|1, +1\rangle$  (blue) and  $|1, -1\rangle$  (red), coupled via coherent radiation with strength  $\Omega_R$ . **b**, Local evolution of the system, represented on the Bloch sphere in the center (where interactions  $\kappa S_z$  exceed the coupling  $\Omega_R$ ) and in the tails (where the coupling exceeds the interaction term). **c**, Pictorial view of the magnetic analogue. The material has a spatially varying ferromagnetic anisotropy  $\gamma$ , smaller or larger than the external magnetic field  $\mathbf{B}$ , respectively on the external or internal regions. The equilibrium magnetization of the material (grey arrow) follows the dominating effect between intrinsic anisotropy and external field. Magnetic domain walls are present at the interface between these regions. Black arrows in panel **b** represent the contributions of the different physical quantities both for the atomic system (top) and for its magnetic analogue (bottom).

the vector on the Bloch sphere (Fig. 1b). The precession happens around a direction that depends on the local properties. While standard magnetic materials quickly align along one axis (grey vector in Fig. 1c) because of dissipation, our nondissipative atomic system allows to study a longer dynamical evolution.

The atomic gas can be described with a two-component order parameter  $\Psi(x) = (\psi_{+1}, \psi_{-1})^T$ , where  $\psi_\alpha$  is the macroscopic wave function of the Bose-Einstein condensate in the state  $\alpha = \pm 1$ . The tight confinement along two spatial directions makes the spatial dynamics to be essentially one-dimensional along the  $x$  direction (see Methods). Therefore, the state of the system is fully described by the density matrix  $(\Psi^* \otimes \Psi)(x) = \{\psi_\alpha^*(x)\psi_\beta(x)\}_{\alpha,\beta=\pm 1}$ . The density matrix is composed by a scalar part,  $n = \text{Tr}(\Psi^* \otimes \Psi)$ , corresponding to the total density of the condensate, and by the spin-density  $\mathbf{s} = \text{Tr}(\boldsymbol{\sigma}\Psi^* \otimes \Psi)$ , with  $|\mathbf{s}| = n$  and  $\boldsymbol{\sigma}$  representing the vector of Pauli matrices. Hereafter vector quantities are defined in the Bloch sphere (see Fig. 1b).

In general the dynamics is described by coupled differential equations for  $n$ ,  $\mathbf{s}$  and the velocity field  $v = j/n$ , where  $j$  is the atom density current. Since the total atom number is a conserved quantity,  $n$  satisfies the continuity equation, with the purely advective current  $j$ :  $\dot{n} + \partial_x j = 0$ . The equation of motion of  $\mathbf{s}$  reflects the possibility of twisting the spin and the absence of spin conservation, both features due to the combination of the coherent Rabi coupling and the lack of SU(2) symmetry of the non-driven system. The Rabi coupling is described by the linear transverse field  $\Omega_R \hat{x}$ . The lack of SU(2) symmetry leads to a nonlinear field  $\kappa s_z \hat{z}$ , with  $\kappa$  proportional to the difference between intra- and intercomponent interactions,  $\delta g$ , and including the effect of the dimensional reduction. The spin equation of motion can be written as

$$\dot{\mathbf{s}} + \partial_x \mathbf{j}_s = \mathbf{H}(\mathbf{s}) \times \mathbf{s}, \quad (1)$$

where we introduce the effective magnetic field  $\mathbf{H} = \Omega_R \hat{x} + \kappa s_z \hat{z}$ . The spin current

$$\mathbf{j}_s = v\mathbf{s} + \frac{\hbar}{2mn} \partial_x \mathbf{s} \times \mathbf{s} \quad (2)$$

is composed of two terms: the first corresponds to the spin advection, while the second is the *quantum torque*, which depends on the atomic mass  $m$ . Remarkably, the quantum torque originates as a pure quantum effect, vanishing when  $\hbar$  is set to zero, or equivalently when the atoms cannot move (see classical analogue in Ref.[8]).

The equation of motion for the spin density, Eq.(1), in the absence of spin advection, is equivalent to a non-dissipative LLE. Therefore, if the density and velocity dynamics can be neglected, the dynamics of a coherently-coupled Bose gas mimics the magnetization dynamics in a magnetic sample, where the quantum torque plays the

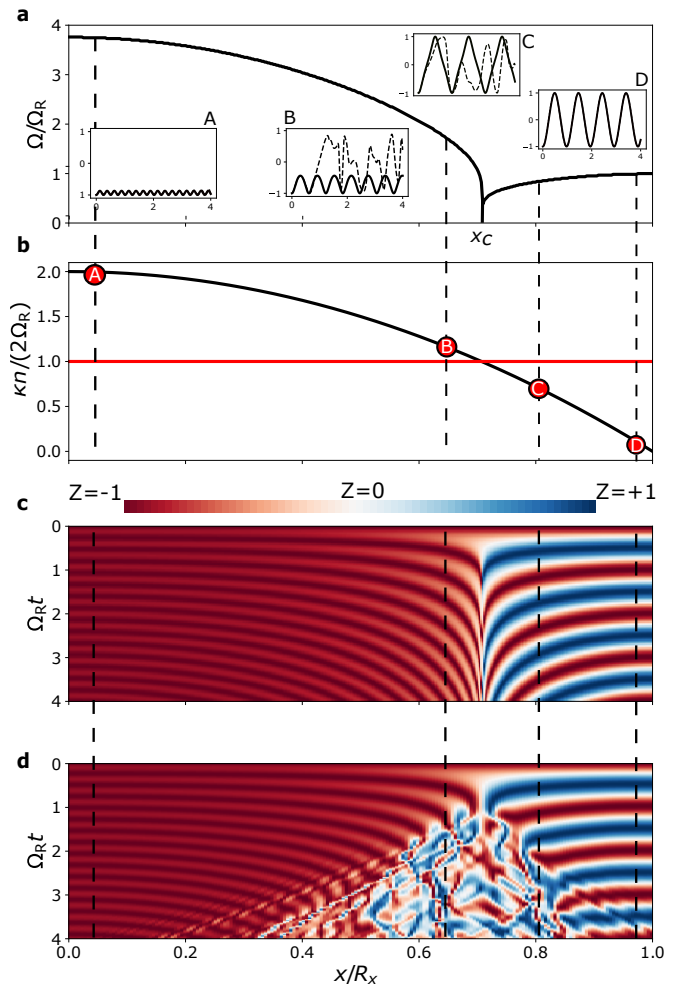


FIG. 2. **Quantum torque effect at the domain wall.** **a**, Main local oscillation frequency  $\Omega$  of the relative magnetization  $Z$  as a function of the position in the gas. The insets show the time evolution of  $Z(t)$  for four different spatial points. **b**, Spatial variation of the magnetic anisotropy. The red line marks the critical value. **c-d**, Time evolution of the magnetization across the cloud according to LLE without (**c**) and with (**d**) quantum torque contribution. Four different spatial points are considered: deep in the self-trapped regime (A), weakly self-trapped (B), weakly oscillating regime (C) and deep in the oscillating regime (D). Continuous and dashed lines in the inset of **a** correspond to the time evolution without and with the quantum torque term, respectively. Note that in B and C, coherence is lost due to the excitation of short wavelength magnetic waves just after a few Rabi periods. In all figures, time, frequency and energy units are related to  $\Omega_R$ . The spatial unit is  $R_x$ .

role of the exchange term. Since the quantum torque depends on the gradient of  $\mathbf{s}$ , it plays a crucial role in the presence of magnetic interfaces. Often in literature the effective field in the LLE includes the torque as well.

Taking advantage of the absence of dissipative terms in Eq. (1), we study the long time dynamics of systems with far-from-equilibrium initial configurations. Before

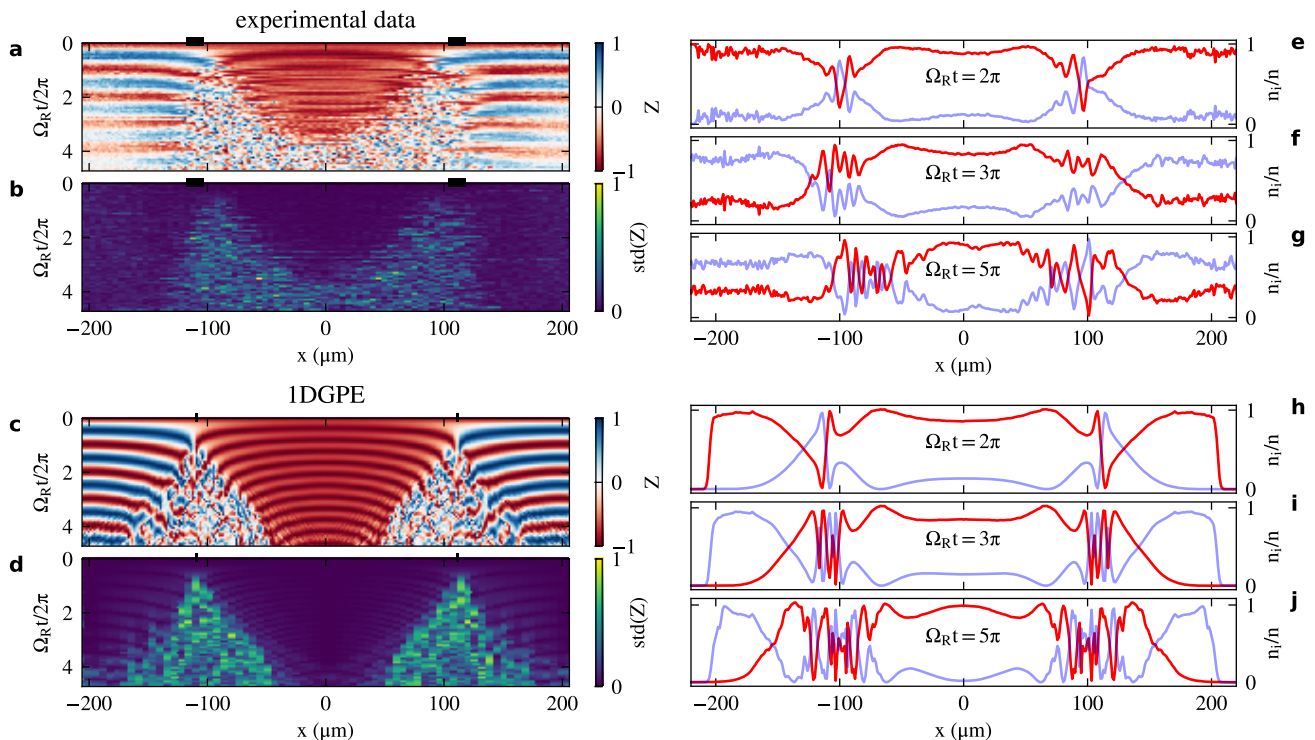


FIG. 3. **Evolution of the magnetization.** **a**, Measured magnetization along the non-uniform 1D gas as a function of time in the presence of a small coupling ( $\Omega_R = 2\pi \times 118 \text{ Hz} = 0.67 \Omega_c$ ). **b**, Standard deviation of the magnetization for spatial windows of  $5 \mu\text{m}$ . Panels **c** and **d** show a numerical Gross-Pitaevskii simulation of the same system. At the interface, around the critical position  $x_c$  (black bars), we observe a net change in the behavior from the oscillating to the self-trapped regime. The width of the bars is evaluated considering the uncertainties in the  $n$  and  $R_x$ . Both regimes break creating a growing region with a strong fluctuation of the magnetization. **e-g**, Measured density profile of each component, normalized to the local total density, for  $\Omega_R t = 2\pi, 3\pi$  and  $5\pi$ . **h-j**, Same as **e-g**, but evaluated numerically.

discussing the actual experimental configuration (Fig. 1a), it is useful to consider the case of a simple spatially homogeneous dynamics. Equation (1) reduces to  $\dot{\mathbf{s}} = \mathbf{H}(\mathbf{s}) \times \mathbf{s}$ , i.e., equivalent to the Josephson equations for weakly-interacting Bose gases [7]. These equations are usually written in terms of the relative magnetization  $Z = s_z/n$  and the relative phase  $\phi = \arctan(s_y/s_x)$ , which in Fig. 1b correspond to the projection of the quantum state on the  $z$  axis of the Bloch sphere, and its equatorial angle, respectively [9], i.e.,  $\mathbf{s} = n(\sqrt{1-Z^2} \cos \phi, \sqrt{1-Z^2} \sin \phi, Z)$ . It is well known that the Josephson model has different dynamical regimes depending on the effective field  $\mathbf{H}$ , as well as on the initial orientation of the spin. In particular, for the initially fully polarized state  $s_z = -n$ , the system can behave in two different ways: (i) for  $\Omega_R > \Omega_c \equiv |\kappa n/2|$ , the magnetization oscillates between  $s_z = \pm n$  with a frequency  $\Omega$  (see the dynamics in C and D in Fig. 2b and associated continuous line in insets), a.k.a. Josephson oscillations; (ii) for  $\Omega_R < \Omega_c$ , the system enters the so-called self-trapped regime [7, 10], where the spin precesses such that  $-n \leq s_z(t) \leq \max(s_z) < 0$ . In the self-trapped regime,  $Z$  never changes sign (see the dynamics in A and

B in Fig. 2b). Interestingly, the precession frequency – not only the amplitude – drastically changes across the transition, as shown in Fig. 2a, with a softening of the precession frequency at the transition point.

The non-homogeneous density of the trapped gas allows us to study the case in which a single system presents both behaviors in spatially different regions. The density profile of our harmonically trapped sample,  $n(x) \propto (1 - x^2/R_x^2)$ , is shown in Fig. 2b (black line). If the central density  $n_0$  is large enough for the system to be locally in the self-trapped regime, there exists a position  $x_c$  that separates this region from the low-density one, where Rabi-like oscillations of the magnetization occur. Other systems of atomic mixtures have been studied in this context, but none showed the possibility to observe both regions in a single sample and the domain wall separating them. Either self-trapped or oscillating regime were observed in "zero"-dimensional (single mode) systems both with Rabi- and tunnel-coupling [10–13]. Spatially extended systems were also studied [14–21], but the entire system was fully in either one or the other regime.

Applying Eq. 1 to an initially fully polarized state,  $|1, -1\rangle$ , which is far from the ferromagnetic uniform

ground state, we observe the spontaneous formation of magnetic domain walls separating regions in which the external field dominates the dynamics from regions where the anisotropy exceeds the external field. Figures 2c and 2d show the theoretical evolution of the magnetization throughout the sample, respectively without and with the quantum torque term, starting from a fully polarized sample with  $s_z(x, t = 0) = -n(x)$ . In the former case, the magnetization develops a strong gradient at the interface between the two regions and this model no longer describes well the system. In fact, the strong gradient triggers the quantum torque to counteract the accumulation of magnetization with an effective field  $-\hbar\partial_x(\partial_x\mathbf{s}/[2mn(x)])$ . Eventually, this breaks the magnetic domain walls and short-wavelength, strongly-polarized magnetic waves are emitted. These waves penetrate the two regions, therefore breaking the local Josephson dynamics, as illustrated in the simulation in Fig. 2d.

Figure 3a shows the experimental measurement of the magnetization. We let the system evolve in the presence of coherent coupling with  $\Omega_R = 0.67\Omega_c$  for a variable time  $t$  and we separately image the two spin populations. This allows us to extract the local magnetization (see Methods). For each experimental run we integrate the magnetization of the elongated atomic sample in the radial directions and obtain  $Z(x)$ . Combining the measurements of  $Z(x)$  at different times  $t$ , we reconstruct the full dynamics, as reported in Fig. 3a. As predicted by theory, the system spatially explores two completely different regimes, depending on the ratio between the driving frequency  $\Omega_R$  and the critical one  $\Omega_c$ . At short time we observe the creation of two magnetic domain walls at positions  $\pm x_c$ , where the condition  $\Omega_R = \kappa n(x_c)/2$  is matched. The magnetization in the central region slightly oscillates, never changing sign, while in the outer part atoms undergo full oscillations at a frequency close to  $\Omega_R$ . As time goes on, the domain walls break, the self-trapped region becomes smaller and smaller and strongly fluctuating regions are created and grow in size. Such dynamics are consistent with a simulation of the Gross-Pitaevskii equation starting with the same parameters of the experiment (Fig. 3c). Deep in both the oscillating and self-trapped regions one can see a smooth spatial variation, associated to a rather small standard deviation. In the strongly fluctuating region, instead, the magnetization varies on a very small length scale, as visible also in the measured (Fig. 3e-g) and numerically simulated (Fig. 3h-j) density profiles. Figure 3b and Fig. 3d show the normalized standard deviation from the mean value over  $5\mu\text{m}$ .

In the self-trapped region, where the density is relatively homogeneous, we can determine for each position  $x$  the time at which the standard deviation of the magnetization experiences a quick jump from zero to a nonzero value. The result is shown in Fig. 4 by combining the times obtained for both sides of the sample. The data

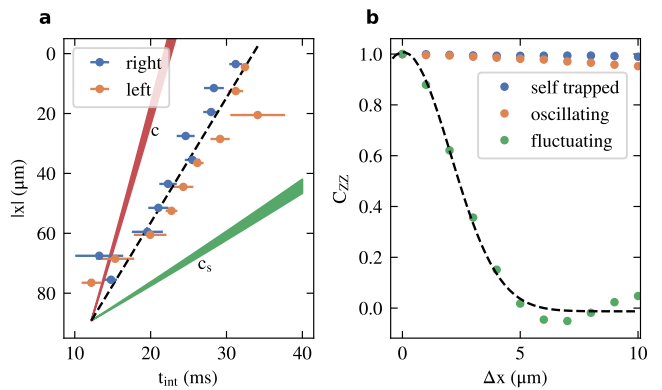


FIG. 4. **Velocity of the breaking front.** **a**, The point where the self-trapped region breaks towards a strongly fluctuating one moves at constant speed across the condensate. The black dashed line is a linear fit corresponding to a velocity  $v = 4.1(1)$  mm/s. The green and red regions show the slope corresponding to the local sound  $c$  and spin sound velocity  $c_s$  considering the uncertainty of  $\kappa n$ . In the plot, the position zero corresponds to the center of the system. Blue and orange dots correspond to the data of the left and right front propagating towards the center, respectively. **Correlation of magnetization.** **b**, We measure the spatial autocorrelation of the magnetization for different regions of the sample. In the self-trapped and oscillating regions, the long-range order of the sample is maintained. In the excited region, the coherence drops to zero at  $\approx 5\mu\text{m}$ .

show a linear behaviour with a speed of the excitation wavefront of  $4.1(1)$  mm/s. In the region where the wavefront propagates, this value is larger than the local spin sound velocity  $c_s \simeq 1.7$  mm/s (green), while it remains well below the local density sound velocity  $c_d \simeq 9.2$  mm/s (red). We estimate the two velocities from  $2mc_s^2 = \hbar\kappa n$ , and  $mc^2 = \hbar\kappa n(g/\delta g)$ , respectively, where  $g$  is the intra-component interaction (see Methods).

The energy accumulated at the domain walls is converted into short-wavelength magnetic waves. Figure 4b shows a measurement of the correlation of the magnetization  $C_{ZZ}(\Delta x)$  given by  $\int s_z(x)s_z(x+\Delta x)/\int s_z(x)^2$ . The magnetization presents no spatial features at short times, while in the fluctuating regime it decays on a length-scale of  $2\mu\text{m}$  (standard deviation of the gaussian fitting function). This value is compatible with the simulations ( $1.6\mu\text{m}$ ), corrected by the finite experimental resolution of the imaging system.

The density profiles (Fig. 3e-j) and the fact that the speed of the magnetic wave front is larger than typical Landau spin critical velocity (Fig. 4), strongly suggest that these excitations are closely related to magnetic shock waves [22–24]. Shock waves have been studied in single component ultracold systems [25, 26] and very recently, in the presence of spin-orbit coupling [27]. However, the LLE in the presence of both transverse magnetic field and anisotropy are not integrable and have

been shown to present a chaotic behavior [28]. Therefore our protocol could excite a new kind of magnetic shock waves with a chaotic character, leading to a turbulent behavior of the magnetization that might have connections with a spin glass. Even on the pure theoretical side, such kind of waves have never been studied and deserve further analysis.

## METHODS

### Experimental procedure

In the experiment, we initially create a polarized Bose-Einstein condensate of up  $5 \times 10^5$  atoms in  $|1, -1\rangle$ . The atoms are trapped in an elongated optical trap [29] with radial and axial frequencies  $\{\omega_x, \omega_r\}/2\pi = \{10(1), 1006(1)\}$  Hz, with Thomas-Fermi radii  $R_r$  and  $R_x$  equal to  $2.2 \mu\text{m}$  and  $210 \mu\text{m}$ , respectively. A stable magnetic field of  $1.3018 \text{ G}$  is applied along the  $z$  axis to lift the degeneracy of the Zeeman substates. We apply a microwave dressing to lift the energy of the  $|1, 0\rangle$  state in order to prevent it from being populated. The high stability and uniformity of the field is ensured by the presence of a 4-layer magnetic shield [30] around the main vacuum cell, that suppresses the field fluctuations by more than 5 orders of magnitude down to  $2 \mu\text{G}$  on the timescale of the full experimental sequence. At the used magnetic field, this corresponds to an energy fluctuation of about  $\approx h \times 3 \text{ Hz}$ . We suddenly switch on a microwave coupling between  $|1, -1\rangle$  and  $|1, +1\rangle$ , by means of a two-photon transition, detuned by  $\Delta$  from the intermediate state  $|2, 0\rangle$ . The strength of the effective Rabi coupling  $\Omega_R$  is tuned by changing  $\Delta$ . The coupled states possess the peculiar feature that the intracomponent coupling constants  $g_{-1} = g_{+1} = g$ , while the interspecies one  $g_{+1, -1}$  is 7% smaller than  $g$  [31]. This leads to a positive  $\kappa$  and miscibility [32, 33]. Our initial condition  $\mathbf{s} = (0, 0, -n)$  corresponds, in the presence of Rabi coupling, to a highly excited state, far from the equilibrium point  $\mathbf{s} = (n, 0, 0)$ .

### Dimensional reduction

Our sample is three dimensional with a Thomas-Fermi (inverted parabola) density profile. Along the transverse direction there is however no dynamics of the magnetisation and the one dimensional LLE or Gross-Pitaevskii equation properly reproduce the transversally integrated measured spin dynamics. In order to determine the one dimensional interaction parameter  $\kappa$  we measured the plasma oscillation frequency  $\omega_p$ , i.e., the frequency of the small magnetic fluctuations around the ground state  $\mathbf{s} = (n, 0, 0)$ . The latter can be indeed measured with high accuracy lasting for a very long time and can be

directly compared with the simple analytical expression  $\omega_p = \sqrt{\Omega_R(\Omega_R + \kappa n)}$ . By measuring the plasma frequency in the central slice of the trap we extract  $\kappa n(x = 0)$ . This value of  $\kappa n(x = 0)$  is in good agreement with the one obtained from the atom number and trapping frequencies. We checked that with such a value at hand we can reproduce the experimental spatial dependent plasma frequency simply by using the Thomas-Fermi one dimensional density  $n(x) = n(x = 0)(1 - x^2/R_x^2)$ .

## ACKNOWLEDGEMENTS

We thank F. Dalfovo for his critical reading of the manuscript and G. Consolo, D. Go, E. Mendive-Tapia and N. Pavloff for fruitful discussions. We acknowledge funding from INFN through the FISH project, from the European Union's Horizon 2020 Programme through the NAQUAS project of QuantERA ERA-NET Cofund in Quantum Technologies (Grant Agreement No. 731473) and from Provincia Autonoma di Trento. We thank the BEC Center, the Q@TN initiative and QuTip.

## AUTHORS' CONTRIBUTION

A.Recati and G.F. conceived the project. A.F. performed the experiment. A.F. and A.Z. analyzed the experimental data. D.T. set up the experiment control. A.G., A.Recati and A.Roy developed the theory and performed the corresponding numerical simulations. A.Recati, A.Z., and G.L. wrote the manuscript. All authors contributed to the discussion and interpretation of the results.

\* Correspondence to  
[giacomo.lamporesi@ino.cnr.it](mailto:giacomo.lamporesi@ino.cnr.it)  
[alessio.recati@ino.cnr.it](mailto:alessio.recati@ino.cnr.it)  
[alessandro.zenesini@ino.cnr.it](mailto:alessandro.zenesini@ino.cnr.it)

† Current address: CNR Nanotec, Institute of Nanotechnology, via Monteroni, 73100, Lecce, Italy.

- 
- [1] H. Zabel and S. D. Bader, (Eds.), *Magnetic Heterostructures: Advances and Perspectives in Spinstructures and Spintransport* (Springer).
  - [2] S. A. Wolf, D. D. Awschalom, R. A. Buhrman, J. M. Daughton, S. von Molnár, M. L. Roukes, A. Y.

- Chtchelkanova, and D. M. Treger, *Science* **294**, 1488 (2001).
- [3] N. Locatelli, V. Cros, and J. Grollier, *Nature Materials* **13**, 11 (2014).
- [4] L. Landau and E. Lifshitz, *Phys. Z. Sowjetunion* **8**, 153.
- [5] V. G. Bar'yakhtar and B. A. Ivanov, *Low Temperature Physics* **41**, 663 (2015).
- [6] B. D. Josephson, *Phys. Lett.* **1**, 252 (1962).
- [7] A. Smerzi, S. Fantoni, S. Giovanazzi, and S. R. Shenoy, *Phys. Rev. Lett.* **79**, 4950 (1997).
- [8] M. Pigneur, T. Berrada, M. Bonneau, T. Schumm, E. Demler, and J. Schmiedmayer, *Phys. Rev. Lett.* **120**, 173601 (2018).
- [9] T. Nikuni, J. E. Williams, and C. W. Clark, *Phys. Rev. A* **66**, 043411 (2002).
- [10] T. Zibold, E. Nicklas, C. Gross, and M. K. Oberthaler, *Phys. Rev. Lett.* **105**, 204101 (2010).
- [11] M. Albiez, R. Gati, J. Fölling, S. Hunsmann, M. Cristiani, and M. K. Oberthaler, *Phys. Rev. Lett.* **95**, 010402 (2005).
- [12] D. Jacob, L. Shao, V. Corre, T. Zibold, L. De Sarlo, E. Mimoun, J. Dalibard, and F. Gerbier, *Phys. Rev. A* **86**, 061601 (2012).
- [13] T. Zibold, V. Corre, C. Frapolli, A. Invernizzi, J. Dalibard, and F. Gerbier, *Phys. Rev. A* **93**, 023614 (2016).
- [14] M. R. Matthews, B. P. Anderson, P. C. Haljan, D. S. Hall, M. J. Holland, J. E. Williams, C. E. Wieman, and E. A. Cornell, *Phys. Rev. Lett.* **83**, 3358 (1999).
- [15] E. Nicklas, H. Strobel, T. Zibold, C. Gross, B. A. Malomed, P. G. Kevrekidis, and M. K. Oberthaler, *Phys. Rev. Lett.* **107**, 193001 (2011).
- [16] S. Levy, E. Lahoud, I. Shomroni, and J. Steinhauer, *Nature* **449**, 579 (2007).
- [17] L. J. LeBlanc, A. B. Bardon, J. McKeever, M. H. T. Extavour, D. Jervis, J. H. Thywissen, F. Piazza, and A. Smerzi, *Phys. Rev. Lett.* **106**, 025302 (2011).
- [18] G. Spagnolli, G. Semeghini, L. Masi, G. Ferioli, A. Trenkwalder, S. Coop, M. Landini, L. Pezzè, G. Modugno, M. Inguscio, A. Smerzi, and M. Fattori, *Phys. Rev. Lett.* **118**, 230403 (2017).
- [19] M. Pigneur and J. Schmiedmayer, *Phys. Rev. A* **98**, 063632 (2018).
- [20] N. Luick, L. Sobirey, M. Bohlen, V. P. Singh, L. Mathey, T. Lompe, and H. Moritz, *Science* **369**, 89 (2020).
- [21] W. J. Kwon, G. Del Pace, R. Panza, M. Inguscio, W. Zwerger, M. Zaccanti, F. Scazza, and G. Roati, *Science* **369**, 84 (2020).
- [22] A. Kosevich, B. Ivanov, and A. Kovalev, *Physics Reports* **194**, 117 (1990).
- [23] T. Congy, A. M. Kamchatnov, and N. Pavloff, *SciPost Phys.* **1**, 006 (2016).
- [24] S. K. Ivanov, A. M. Kamchatnov, T. Congy, and N. Pavloff, *Phys. Rev. E* **96**, 062202 (2017).
- [25] J. J. Chang, P. Engels, and M. A. Hoefer, *Phys. Rev. Lett.* **101**, 170404 (2008).
- [26] M. E. Mossman, M. A. Hoefer, K. Julien, P. G. Kevrekidis, and P. Engels, *Nature Communications* **9**, 4665 (2018).
- [27] M. E. Mossman, E. S. Delikatny, M. M. Forbes, and P. Engels, "Shock waves in a superfluid with higher-order dispersion," (2020), [arXiv:2004.00832](https://arxiv.org/abs/2004.00832) [cond-mat.quant-gas].
- [28] M. Daniel, M. D. Kruskal, M. Lakshmanan, and K. Nakamura, *Journal of Mathematical Physics* **33**, 771 (1992).
- [29] A. Farolfi, D. Trypogeorgos, C. Mordini, G. Lamporesi, and G. Ferrari, *Phys. Rev. Lett.* **125**, 030401 (2020).
- [30] A. Farolfi, D. Trypogeorgos, G. Colzi, E. Fava, G. Lamporesi, and G. Ferrari, *Review of Scientific Instruments* **90**, 115114 (2019).
- [31] S. Knoop, T. Schuster, R. Scelle, A. Trautmann, J. Appmeier, M. K. Oberthaler, E. Tiesinga, and E. Tiemann, *Phys. Rev. A* **83**, 042704 (2011).
- [32] T. Bienaimé, E. Fava, G. Colzi, C. Mordini, S. Serafini, C. Qu, S. Stringari, G. Lamporesi, and G. Ferrari, *Phys. Rev. A* **94**, 063652 (2016).
- [33] E. Fava, T. Bienaimé, C. Mordini, G. Colzi, C. Qu, S. Stringari, G. Lamporesi, and G. Ferrari, *Phys. Rev. Lett.* **120**, 170401 (2018).